Second-order robust regularization cost function for detecting and reconstructing phase discontinuities

Carlos Galvan and Mariano Rivera

We propose a robust method for computing discontinuous phase maps from a fringe pattern with carrier frequency. Our algorithm is based on the minimization of an edge-preserving regularized cost function, specifically, on a robust regularized potential that uses a paradigm called the plate with adaptive rest condition, i.e., a second-order edge-preserving potential. Given that the proposed cost function is not convex, our method uses as its initial point an overly smoothed phase computed with a standard fringe analysis method and then reconstructs the phase discontinuities. Although the method is general purpose, it is introduced in the context of interferometric gauge-block calibration. The performance of the algorithm is demonstrated by numerical experiments with both synthetic and real data.

OCIS codes: 120.265, 0120.3180, 120.3940, 120.6650, 100.3190.

1. Introduction

Phase recovery from discontinuous fringe patterns is a challenging issue that is relevant when phase-stepping methods of phase recovery are not applicable because of transience of either a studio object or the illumination. In this paper we present a general algorithm for computing discontinuous phases and illumination-component maps. Given that the proposed cost function is not quadratic, our method uses as its starting point the unwrapped phase[1,2] of the phase computed with a standard fringe-analysis algorithm (for instance, that proposed by Takeda *et al.*[3] or by Womack[4]). Such an initial phase has overly smoothed phase discontinuities and a residual tilt product of the remaining carrier frequency. The proposed method detects the phase discontinuities and reconstructs the discontinuous phase. Our algorithm can be applied when a good approximation of the discontinuous phase is available. In this sense our method is closely related to a phase-refinement method recently reported by Rivera[5]; however, in this paper we focus on the detection and reconstruction of phase discontinuities.

We use as a studio case interferograms observed during calibration of gauge blocks (GBs).[6–8] The GB calibration task is performed by interferometric means by primary metrology laboratories, e.g., the National Institute of Standards and Technology in the United States of America, the National Research Council in Canada, the National Physical Laboratory in the United Kingdom, and the Centro Nacional de Metrologia (CENAM) in Mexico.

Calibration of GBs is the first step in the chain of establishing a length standard, e.g., the meter, which is the only primary length standard determined with higher precision than the GB. This highly precise calibration task is performed with optical interferometers that have been previously calibrated with respect to the primary length standard. The primary GBs, optically calibrated, are used as standards for calibrating other GBs. That less-precise secondary calibration is performed with mechanical comparators.

In this paper we examine the calibration of GBs by interferometric techniques. Specifically, we present an algorithm for phase retrieval from a single interferogram of GBs. In Fig. 1 we show interferograms that correspond to GBs of different materials, namely, tungsten carbide [Fig. 1(a)] and steel [Fig. 1(b)]. These fringe patterns were obtained from the video signal of the GB interferometer at the CENAM; this explains the spurious column shift in the image. Such an interferometer is a commercial instrument based on a

C. Galvan (cgalvan@cenam.mx) is with the Centro Nacional de Metrologia Apartado Postal 1-100 Centro, Queretaro, Queretaro, Mexico 76000. M. Rivera (mrivera@cimat.mx) is with the Centro de Investigacion en Matematicas A. C., Apartado Postal 402, Guanajuato, Guanajuato, Mexico 36000.

Received 14 April 2005; revised 28 July 2005; accepted 28 July 2005.

0003-6935/06/020353-07$15.00/0

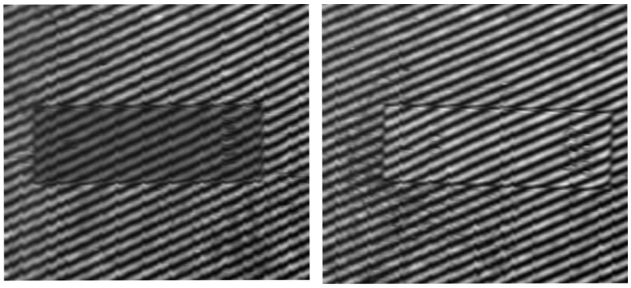

Fig. 1. Interferograms of a GB on a steel plate: (a) tungsten carbide, (b) steel.

Twyman–Green setup with two laser beams of two wavelengths, 633 and 543 nm. The procedure for estimating the GB's length was described by Pugh and Jackson,[6] and it is briefly described here as follows: The GBs to be measured are wrung onto a lapped reference plate and positioned in the interferometer such that open fringes across the GB and the plate are observed. The fringe pattern's spatial frequency is controlled by a piezo nanoactuator (piezoelectric transducer) that produces a tilt of the reference mirror. The GB introduces fringe displacements in the GB region with respect to the fringes in the plate region. Such relative fringe displacements are known as fringe fractions. A coarse measure of the GB's length is computed from the relative phase between the interferograms that correspond to 633 and those to 543 nm wavelengths. These GB lengths are computed with limited precision, with an error of ± 1.5 μm with respect to the true length. In a second stage, the initial measure is improved with the high-precision phase map computed from the interferogram that corresponds to 543 nm (Fig. 1). Unfortunately, if one uses standard fringe-analysis algorithms for estimating the correction phase map, the phase discontinuity between the GB and the plate will be overly smoothed, i.e., the correction phase map will be corrupted.

We present a fringe-analysis method for interferograms with frequency carriers that recovers discontinuous phase maps such as those shown in Fig. 1. Such interferograms can be represented by the observation model (or direct model)

$$g_r = \hat{a}_r + \hat{b}_r \cos(\hat{\omega}^{\mathrm{T}} r + \hat{\phi}_r) + \eta_r, \qquad (1)$$

where $r = [x,\ y]^{\mathrm{T}}$ represents the position of pixel r in regular lattice L; $\hat{a}$ and $\hat{b}$ are the background and contrast illumination components, respectively; $\hat{\omega} = [\hat{\omega}_x,\ \hat{\omega}_y]^{\mathrm{T}}$ is the spatial carrier frequency; $\hat{\phi}$ is the phase; and η represents independent additive noise introduced in the image at the time of acquisition. Our task is to compute an estimation ϕ of phase map $\hat{\phi}$ for each pixel of the fringe pattern. Based on *a priori* knowledge of the experimental setup, we can establish the following conditions:

(a) The illumination components (background and contrast) are piecewise smooth because the elements in the image (reference plate and GB) may be composed of different materials.

(b) The phase is piecewise smooth because of the GB.

(c) Carrier frequency $\hat{\omega}$ is constant, but its precise value is unknown. However, an estimation ω of the carrier can be computed. Moreover, the carrier frequency has been chosen in such a way that an open fringe interferogram is observed.

Here *a priori* knowledge needs to (and must) be taken into account if one is to effectively recover the phase, $\hat{\phi}$, from an interferogram of a GB. For such a purpose, in the past decade several authors have proposed methods that use regularization techniques[9] such as quadrature filters,[10] adaptive quadrature filters,[11] and robust cost functions.[5,12] But such methods take into account neither illumination components nor phase discontinuities. Herein we propose a method for computing an estimation, ϕ, of fractional displacement $\hat{\phi}$ of the fringe pattern in the GB calibration task, given fringe pattern g and an estimation of the carrier frequency, ω. To solve such an inverse problem we minimize a regularized cost function of the general form[13]

$$U(a,\ b,\ \phi,\ l; g,\ \omega) = D(a,\ b,\ \phi;\ g,\ \omega) + \lambda R(a,\ b,\ \phi,\ l), \qquad (2)$$

in which the first term on the right-hand side, D, is known as the data term and promotes fidelity of the computed variables to the observed data; i.e., the estimated phase and illumination components (ϕ and a, b, respectively) should be consistent with observed data g and estimated frequency ω, according to the model in Eq. (1). Note that we propose the joint estimation of the phase and the illumination components. The term, R, codifies our *a priori* information, i.e., *a priori* conditions (a)–(c) expressed above, for the solution. Generally, the regularization term is expressed as a potential that promotes smooth solutions. Finally, field l acts as a phase-discontinuity indicator map. Given that the phase-discontinuity locations are not known in advance, our method also estimates edge-detector field l.

The paper is organized as follows: In Section 2 we present a review of the regularization method based on the plate with adaptive rest condition (PARC) paradigm[12] (PARC potentials). Such a method is a second-order edge-preserving regularization method that deals naturally with first- and second-order discontinuities: steps and slope breaks, respectively. In Section 3 we present our method for analysis of a discontinuous fringe pattern. The method is based on the minimization of a regularized cost function with PARC potentials, and it includes the joint estimation of the illumination components. In Section 4 we describe experiments with both synthetic and real data

that demonstrate the method's performance. Finally, our conclusions are presented in Section 5.

2. Regularization Using PARC Potentials

Bayesian regularization, based on Markov random fields theory,[13] is a general and well-accepted theoretical framework for solving inverse problems in image-processing tasks. Such a theory has been effective for formulating algorithms for solving such fringe-analysis problem as fringe filtering,[10,11] closed fringe analysis,[5,14,15] phase unwrapping,[1,2,16,17] and phase stepping.[2,18] In the Markov random fields framework the data term in Eq. (2) is formulated as a negative log likelihood that depends on the observation model [Eq. (1)] and on the noise distribution.[13] Therefore assuming that noise η has a Gaussian-independent identical distribution yields the data term

$$D(a,\ b,\ \phi;\ g,\ \omega) = \sum_{r \in L} \left[g_r - a_r - b_r \cos(\omega^{\mathrm{T}} r + \phi_r)\right]^2. \tag{3}$$

Regularization term R, however, must be expressed in a form such that a penalty is imposed for violation of *a priori* knowledge conditions (a)–(c) above.

To choose the correct form of the regularization term, we establish the next condition: Robust regularized methods for image restoration based on first-order potentials (i.e., in the adaptive membrane) promote flat (almost constant) reconstructions.[12,19–23] Those potentials are of the form

$$R(\phi,\ l) = \sum_{\langle rs \rangle} \left[(\phi_r - \phi_s)^2 {l_{rs}}^2 + \Phi(l_{rs})\right], \tag{4}$$

where convex potential $\Phi(\ )$ controls the detection of discontinuities and $\langle rs \rangle$ are sets (cliques in the jargon of Markov random fields) of first-neighbor pixel pairs, i.e., $\langle rs \rangle \in c = [(r, s): r, s \in L, |r - s| < 2]$. It is well known that first-order edge-preserving regularization potentials tend to underestimate slopes in the restored image. This underestimation produces a flatness of the slopes and introduces artificial edges into large slopes: This is the well-known staircase effect.[12,20,24,25] It is a limitation of first-order edge-preserving regularization potentials in fringe analysis because, if the carrier frequency is estimated with a limited accuracy, then the residual carrier appears as a remaining constant slope in the phase. Second-order regularization terms (the thin-plate model), however, are expressed as the summation of quadratic potentials. Such a summation runs over cliques of pixel triads, $\langle qrs \rangle$, in horizontal, vertical, and diagonal positions[5] (see Fig. 2):

$$R(f) = \sum_{\langle qrs \rangle} (\phi_q - 2\phi_r + \phi_s)^2. \tag{5}$$

In spite of the quadratic potential, Eq. (5) promotes smooth gradient solutions, which tend to overly smooth edges. Therefore Geman and Reynolds were motivated to propose robust second-order potentials,[20] e.g.,

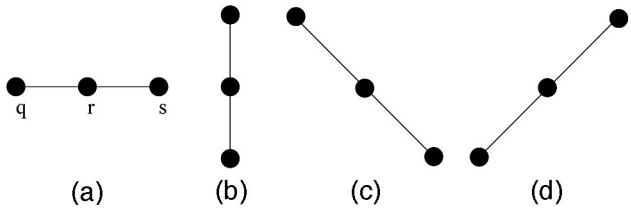

Fig. 2. Cliques of pixels in the following positions: (a) horizontal, (b) vertical, and (c), (d) diagonal.

$$R(\phi,\ l) = \sum_{\langle qrs \rangle} \left[(\phi_q - 2\phi_r + \phi_s)^2 {l_{qrs}}^2 + \Phi(l_{qrs})\right], \tag{6}$$

which preserve slope changes. However, it is well known that potential (6) overly smooths steps in ϕ. Recently Rivera and Marroquin[12] proposed a new family of robust second-order potentials: the so-called PARC potentials. PARC potentials can deal with ramps (regions with smooth variations in the intensity gradient) and first-order discontinuities (spatial steps). That is a significant advantage with respect to potentials based on the Geman–Reynolds formulation. In this paper we describe the second-order edge-preserving potentials with an explicit line PARC[12] (PARC-EL). The PARC-EL–based regularization term is expressed as a summation over cliques of size three of the form (Fig. 2)

$$R_3(\phi,\ l) = \sum_{\langle rqs \rangle} \rho_{qrs}(\phi,\ l), \tag{7}$$

with the PARC-EL potential $\rho_{qrs}(\phi, l)$ defined by

$$\rho_{qrs}(\phi,\ l) = (l_{qr}\,\Delta\phi_{qr} - l_{rs}\Delta\phi_{rs})^2 + \mu[(1 - l_{qr})^2 + (1 - l_{rs})^2], \tag{8}$$

where we define $\Delta\phi_{qr} \overset{\text{def}}{=} \phi_q - \phi_r$, $\Delta\phi_{rs}$ is defined in a similar way, and l_{rs} acts as a first- and second-order discontinuity detector; i.e., l_{rs} is close to zero if there is a step or an abrupt change in the ϕ slope of the first-neighbor pixel pair $\langle r, s \rangle$.

The behavior of the PARC-EL potential is explained as follows: The contribution of the regularization term is computed as a compromise between the two terms in Eq. (8) whose relative contributions are controlled by positive parameter μ; depending on the values of the local differences $\Delta\phi_{qr}$ and $\Delta\phi_{rs}$ PARC-EL potentials perform any of three regularizations:

(a) Second-order smoothness. If the thin-plate potential is relatively small, $|\Delta\phi_{qr} - \Delta\phi_{rs}| < 2\mu$, the minimum cost is achieved with $l_{qr} \approx 1$ and $l_{rs} \approx 1$. This implies first-order smoothness: $|\Delta\phi_{qr}| < \mu$ and $|\Delta\phi_{rs}| < \mu$.

(b) Preservation of second-order discontinuities. For large-plate potential values, e.g., $|\Delta\phi_{qr} - \Delta\phi_{rs}|$

$> 2\mu$, with $|\Delta\phi_{qr}| > \mu$ and $|\Delta\phi_{rs}| > \mu$; the PARC-EL potential behaves as the Geman–Reynolds robust potential [Eq. (6)], and the minimum cost (close to 2μ) is achieved with $l_{qr} \approx 0$ and $l_{rs} \approx 0$.

(c) Preservation of first-order-discontinuities. For $|\Delta\phi_{qr}| < \mu$ and $|\Delta\phi_{rs}| > \mu$, the PARC-EL potential becomes robust to the largest difference; i.e., the minimum potential cost is obtained with $l_{qr} \approx 1$ and $l_{rs} \approx 0$. When $|\Delta\phi_{qr}| > \mu$ and $|\Delta\phi_{rs}| < \mu$, the PARC-EL potential has a similar behavior and the minimum cost is obtained with $l_{qr} \approx 0$ and $l_{rs} \approx 1$.

In Section 3 below, we present the complete function for phase recovery with second-order discontinuities.

3. Edge-Preserving Function for Fringe Analysis Based on PARC-EL Potentials

Carrier frequency $\hat{\omega} = [\hat{\omega}_x, \hat{\omega}_y]^T$ in Eq. (1) can be estimated with limited precision. Because of such a residual error, standard fringe-analysis methods[3,4] introduce a constant slope of ϕ° into the recovered (estimated) phase. Moreover, given that the standard fringe-analysis algorithms mentioned above (of Takeda *et al.*[3] and Womack[4]) assume limited bandwidth phases (smooth phases), the real phase discontinuities will be overly smoothed. We have proposed using ϕ° as an initial phase (starting point) and then detecting and reconstructing the phase discontinuities. For such a purpose we use PARC-EL potentials in regularization term R to recover piecewise smooth-sloped phase maps. Moreover, we assume that illumination-components' discontinuities coincide with phase discontinuities (Fig. 1). So phase and illumination steps are coupled in the PARC-EL potential by a unique edge-detector field, l. Therefore we propose to compute the phase and the illumination components by minimizing the cost function:

$$\begin{aligned} U(a,\ b,\ \phi,\ l) = \sum_r \left[g_r - a_r - b_r \cos(\omega^T r + \phi_r)\right]^2 \\ + \sum_{\langle q,\ r,\ s\rangle} \{\lambda_a (l_{qr}\Delta a_{qr} - l_{rs}\Delta a_{rs})^2 \\ + \lambda_b (l_{qr}\Delta b_{qr} - l_{rs}\Delta b_{rs})^2 + \lambda_c (l_{qr}\Delta\phi_{qr} \\ - l_{rs}\Delta\phi_{rs})^2 + \mu[(1 - l_{qr})^2 + (1 - l_{rs})^2]\}, \end{aligned} \tag{9}$$

where positive regularization parameter, λ_a, λ_b, λ_c, and μ control the relative contribution of each term to the total cost. The minimization of Eq. (9) is performed by alternating minimizations with respect to ϕ, a, b, and l; such a scheme consists of iterating the algorithm for analysis of discontinuous fringe patterns (ADFP; Appendix A) until it converges.

In the research reported here we compute an estimation, $\omega = [\omega_x, \omega_y]^T$, of the fringe pattern's carrier frequency with the method reported by Huntley.[26] Note that, because of the cosine function, minimization with respect to phase ϕ^{k+1} (step 1 of the ADFP algorithm) leads us to the solution of a nonlinear equation system. For solving such a nonlinear system we use a simple gradient descent algorithm that uses as a starting point the result of the previous step, ϕ^k, i.e., by assuming fixed a^k, b^k, and l^k; then ϕ^{k+1} is computed as the fixed point of the gradient descent iteration:

$$\phi_{i+1}{}^{k+1} = \phi_i{}^{k+1} - \alpha \nabla_\phi U(a^k,\ b^k,\ \phi_i{}^{k+1},\ l^k), \tag{10}$$

where α is the step size, $\phi_0{}^{k+1} = \phi^k$ is the initial guess, and $\nabla_\phi U(a^k, b^k, \phi_i{}^{k+1}, l^k)$ denotes the partial gradient of cost function U with respect to phase ϕ and evaluated at $\phi_i{}^{k+1}$. The initial phase, ϕ^0, is computed with a standard spatial fringe-analysis algorithm.[4,27] Note that, if the initial phase is a homogeneous map equal to 0, the ADFP algorithm computes a wrapped phase; i.e., discontinuities (edges) are introduced at those sites where the phase is wrapped. Additionally, steps 2, 3, and 4 in the ADFP algorithm correspond to performing quadratic minimizations, i.e., to solution of the linear systems: $\nabla_a U(a, b^k, \phi_i{}^{k+1}, l^k) = 0$, $\nabla_b U(a^{k+1}, b, \phi_i{}^{k+1}, l^k) = 0$, and $\nabla_l U(a^{k+1}, b^{k+1}, \phi_i{}^{k+1}, l) = 0$, respectively. Such minimizations can be achieved with standard fast minimization algorithms such as a Gauss–Seidel scheme or the conjugate gradient.[28] More details of the procedure for computing the discontinuities' detector field, l, are given in Appendix B.

The ADFP algorithm requires us to find the exact partial minimization and therefore is computationally inefficient. However, in practice such partial minimizations are not fully achieved but are approximated such that

$$\begin{aligned} U(a^k,\ b^k,\ \phi^k,\ l^k) &\geq U(a^k,\ b^k,\ \phi^{k+1},\ l^k) \\ &\geq U(a^{k+1},\ b^k,\ \phi^{k+1},\ l^k) \\ &\geq U(a^{k+1},\ b^{k+1},\ \phi^{k+1},\ l^k) \\ &\geq U(a^{k+1},\ b^{k+1},\ \phi^{k+1},\ l^{k+1}) \\ &\geq 0 \end{aligned}$$

is satisfied at each iteration. Convergence to at least a local minimum is guaranteed because $U(a, b, \phi, l)$ is bounded by zero.

4. Experiments

In this section we show the results computed with the proposed ADFP algorithm for both synthetic and real data.

The first experiment corresponds to the analysis of one-dimensional synthetic data. Figure 3(a) shows the synthetic data (values of phase and illumination elements a and b) generated by use of the direct observation model [Eq. (1)] and the following settings:

$$a_r = \{0.6 \text{ if } 97 \leq r \leq 165; \quad 1.0 \text{ otherwise}\},$$

$$b_r = \{0.5 \text{ if } 97 \leq r \leq 165; \quad 0.9 \text{ otherwise}\},$$

$$\phi_r = \{1.2 + 0.005r \text{ if } 97 \leq r \leq 165,$$

$$0.2 + 0.005r \quad \text{otherwise}.$$

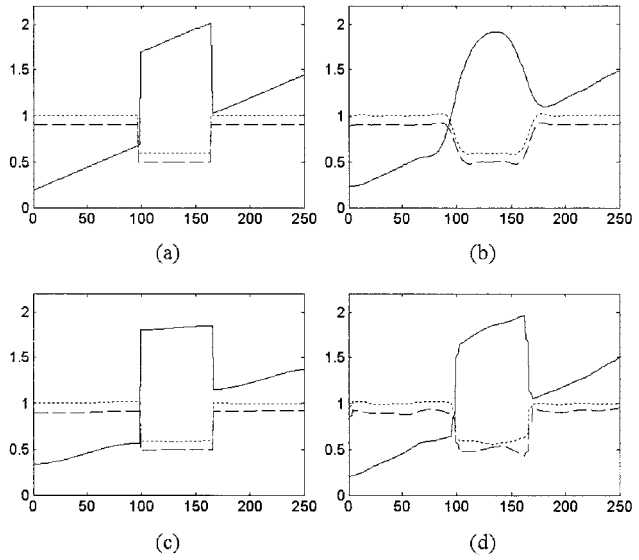

Fig. 3. (a) Synthetic one-dimensional data: phase (continuous curve), background (dashed curve), and contrast (dotted curve). Results computed with (b) a quadratic thin-plate potential, (c) a robust membrane potential, (d) a PARC potential. The original data were corrupted with a white-noise signal with a mean equal to zero and a standard deviation of 0.5 rad.

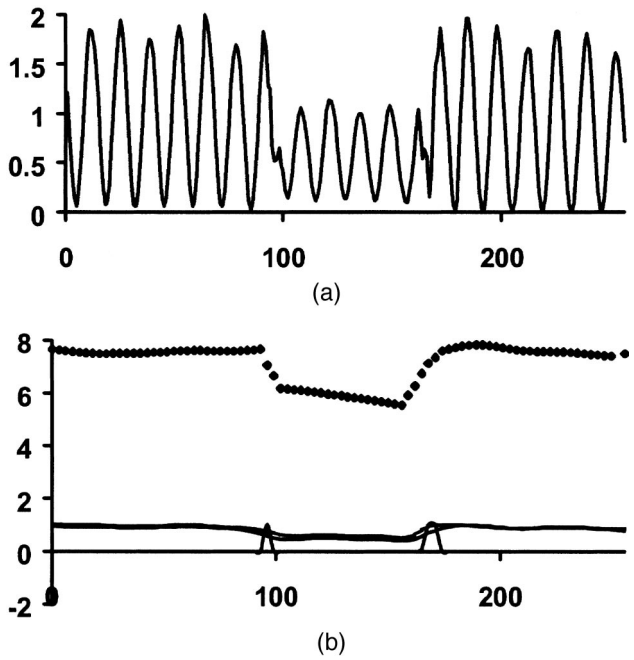

Fig. 4. Real data from the TESA interferometer at CENAM. (a) Central column of the interferogram in Fig. 1. (b) Results computed with the proposed ADFP algorithm: phase (dotted curve), illumination components (solid curves), and edges (markers).

Then the one-dimensional fringe pattern was generated by use of a known frequency ω and corrupted with additive Gaussian noise. The experiments were performed with the real carrier frequencies; however, the phase has a small slope that simulates a residual carrier. Figure 3(b) shows the results computed by use of the nonrobust thin-plate potential [Eq. (5)]. Note the oversmoothness of the phase and the steps in the illumination components. Figure 3(c) shows the results computed by use of first-order edge-preserving potentials and coupling edges of the phase and the illumination components, i.e., Eq. (4) with $\Phi(l_{rs}) = \mu(1 - l_{rs})^2$ and the parameter $\mu = 0.001$ for controlling edge detection. Even though the discontinuities and illumination components have been correctly computed, one can note that the phase slopes are underestimated. It is also well known that first-order edge-preserving potentials introduce spurious edges in large slopes (a staircase effect). Figure 3(d) shows results computed with the proposed method. Table 1 lists the L_2 norm of the error vector of the phase and the illumination components computed by use of the following regularization potentials in Eq. (9): a thin plate [Eq. (4)], a robust membrane [Eq. (5)], and PARC-EL [Eqs. (7) and (8)]. Even though the robust membrane potential computes illumination components accurately (piecewise constant), the phase slope is underestimated. The best phase map (with a piecewise smooth gradient) is computed with PARC-EL potentials. The bottom row in Table 2 shows the computational times for the compared regularized cost functions. We note, as expected, an extra computational cost of the PARC-EL formulation with respect to the quadratic-plate-based formulation, but such a computational cost is not significant if we take the phase improvement into account. Moreover, such computational times can be reduced if, instead of an inefficient simple gradient descent scheme [Eq. (10)], one uses a more-efficient minimization algorithm such as the Newton or Gauss–Newton algorithm.[28]

Figure 4 shows the results computed from one-dimensional real data. In this experiment a tungsten carbide GB was wrung on a steel reference plate, and the interferogram was acquired by the TESA Gauge Block Interferometer at CENAM. The results, shown in Fig. 4(b), show steps (discontinuities) in the phase (dotted curve) and in the illumination (continuous

Table 1. L_2 Error in Results and Computational Times Computed with Three Potentials

	Thin Plate (Quadratic)	Robust Membrane (Half-Quadratic)	Robust Thin Plate (PARC-EL)
Phase (ϕ)	4.9819	1.8936	0.9952
Background (a)	0.4447	0.7123	0.5156
Contrast (b)	0.5122	0.6959	0.7704
Computational time (s)	40	25	51

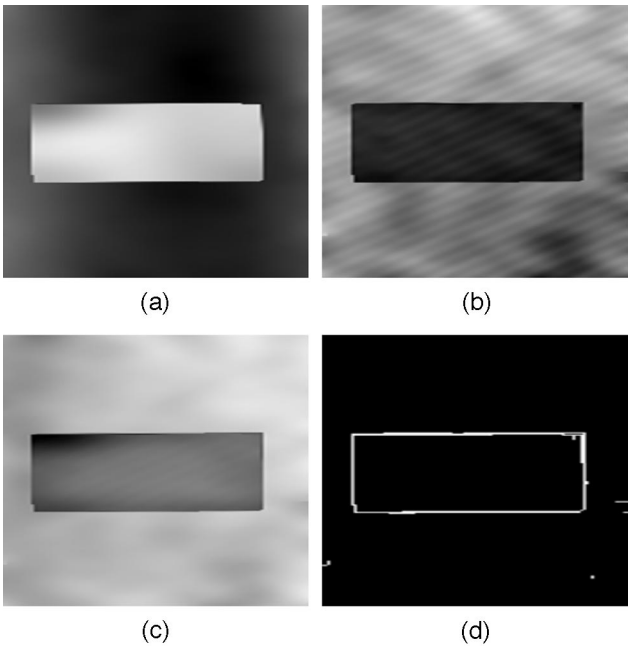

Fig. 5. Two-dimensional fringe-pattern analysis with the proposed ADFP algorithm: (a) phase map, (b) background illumination, (c) contrast component, (d) detected edge map.

curves) components. One can observe a small tilt in the computed phase map in the GB region: Such a tilt may result from incorrect wringing of the GB on the reference plate. One can also note that the edges are not well defined in the data [Fig. 4(a)] and that as consequence sharp discontinuities are not detected; see Fig. 4(b). The quality of such results can be improved by two-dimensional processing of the fringe pattern.

Figure 5 shows the components computed with the proposed method in the two-dimensional fringe pattern shown in Fig. 1(a). Figure 5(a) shows the piecewise phase map with the relative fractional phase between the GB and the reference plate. Figures 5(b) and 5(c) show the background and the contrast components, respectively. Finally, Fig. 5(d) shows the discontinuities map (edges). In this case the computed discontinuities are sharp and are located according to the observed edges in the noisy interferogram [Fig. 1(a)]. The data were not preprocessed to reduce the noise or correct the spurious column shift in the image.

5. Conclusions

We have presented a regularization model for analysis of interferograms with discontinuities. The method estimates the phase map and the illumination components according to an interference equation.

The algorithm presented is a method for detecting and reconstructing the spatial phase discontinuities provided by an initial phase previously computed by a standard method so that, in principle, if an overly smoothed discontinuous phase can be computed from a fringe pattern with (or without) a carrier, our algorithm can be used to detect and restore such phase discontinuities. However, in general, the issue of closed analysis is beyond the scope of the proposed method (the reader can see Ref. 5 for more details about a method that addresses such a problem).

Our algorithm uses as initial data the unwrapped phase computed with a standard fringe-analysis algorithm. Given that such standard algorithms[3,4] assume smooth (limited bandwidth) phase and illumination components, the initial phase has overly smoothed phase discontinuities. We assume that the discontinuity locations are not known in advance, such that they need to be estimated. The proposed method effectively detects and reconstructs the phase discontinuities. The ADFP algorithm presented is based on the minimization of a cost function that uses, as regularization potentials, thin-plate potentials with adaptive rest condition, PARC potentials. PARC potentials constrain the solution to be piecewise with almost constant slopes. PARC potentials allow discontinuous phase maps to be recovered with piecewise smooth gradients, such that they are particularly useful when the carrier frequency is estimated with limited accuracy that allows a residual constant slope to remain in the initial phase.

This research was performed in partial fulfillment of the requirements for a M.Sc. degree by C. Galvan at the Centro de Investigacion en Matematicas and was supported in part by a scholarship from the Consejo Nacional de Ciencia y Tecnologia (CONACYT) and by a grant from the CENAM. The research of M. Rivera was partially supported by the CONACYT grants 40722 and 46270. The authors thank the referees for their comments that helped to improve the quality of the paper.

Appendix A. ADFP Algorithm

1. Choose λ_a, λ_b, λ_c, and μ;
2. Compute an approximation of the carrier frequency, $\omega = [\omega_x, \omega_y]^T$;
3. Set $a_r^0 = 1$, $b_r^0 = 1$, and $l_r^0 = 1$ for all $r \in L$;
4. Compute an initial phase, ϕ_r^0, for all $r \in L$ {by using a standard fringe-analysis method[3,4] and then by unwrapping the computed phase[1,2]}.
5. **For** $k = 0, 1, \ldots$:
6. Compute $\phi^{k+1} = \arg\min_\phi U(a^k, b^k, \phi, l^k)$, using as an initial guess $\phi = \phi^k$;
7. Compute $a^{k+1} = \arg\min_a U(a, b^k, \phi^{k+1}, l^k)$;
8. Compute $b^{k+1} = \arg\min_b U(a^{k+1}, b, \phi^{k+1}, l^k)$;
9. Compute $l^{k+1} = \arg\min_l U(a^{k+1}, b^{k+1}, \phi^{k+1}, l)$;
10. **If** $\|\phi^k - \phi^{k-1}\|_2^2 < \varepsilon$,
11. **STOP**, with solution $(a^{k+1}, b^{k+1}, \phi^{k+1}, l^{k+1})$;
12. **End**

APPENDIX B. Gauss–Seidel Scheme for Computing the Discontinuous Detector Field

The one-dimensional algorithm for computing the discontinuous detection field (step 9 in the ADFP algorithm) is presented. However, this method can straightforwardly be extended to two dimensions. Let

$a,\ b,\ \phi \in \Re^N$ and $l \in \Re^{N-1}$; then we define $\Delta x_i \overset{\text{def}}{=} x_i - x_{i-1}$ for $i = 1,\ 2,\ \ldots,\ N$. Therefore the one-dimensional version of cost function (9) is written as

$$\begin{aligned} U_{1d}(a,\ b,\ \phi,\ l) = Q(a,\ b,\ \phi) + \sum_{i=2}^{N-1} \{ & \lambda_a(l_i \Delta a_i \\ & - l_{i-1}\Delta a_{i-1})^2 + \lambda_b(l_i \Delta b_i - l_{i-1}\Delta b_{i-1})^2 \\ & + \lambda_c(l_i \Delta \phi_i - l_{i-1}\Delta \phi_{i-1})^2 + \mu[(1 - l_i)^2 \\ & + (1 - l_{i-1})^2]\}, \end{aligned}$$

where $Q(a,\ b,\ \phi)$ represents the independent terms of l. Then, from

$$\frac{1}{2}\frac{\partial U_{1d}(a,\ b,\ \phi,\ l)}{\partial l_i} = 0,$$

we have

$$\begin{aligned} & \lambda_a \Delta a_i[(l_i \Delta a_i - l_{i+1}\Delta a_{i+1})W(i+1) \\ & \quad + \lambda_a(l_i \Delta a_i - l_{i-1}\Delta a_{i-1})] + \lambda_b \Delta b_i[(l_i \Delta b_i - l_{i+1}\Delta b_{i+1}) \\ & \quad \times W(i+1) + \lambda_b(l_i \Delta b_i - l_{i-1}\Delta b_{i-1})] \\ & \quad + \lambda_c \Delta \phi_i[(l_i \Delta \phi_i - l_{i+1}\Delta \phi_{i+1})W(i+1) + \lambda_c(l_i \Delta \phi_i \\ & \quad - l_{i-1}\Delta \phi_{i-1})] + \mu(l_i - 1) = 0, \end{aligned} \tag{B1}$$

where $W(x) = (1 \text{ if } x < N - 1;\ 0 \text{ otherwise})$. The Gauss–Seidel scheme corresponds to the solution of Eq. (B1) for l_i, with $a,\ b,\ \phi,$ and $(l_{i+1},\ l_{i-1})$ kept fixed, for $i = 2,\ 3,\ \ldots,\ N$, where l_{i-1} is the previously updated value. Such a procedure is iterated for all the pixels until convergence. Note that edge detector variable l_i is associated with the pair of pixels in the clique $\langle i,\ i - 1\rangle$.

References

1. J. L. Marroquin and M. Rivera, "Quadratic regularization functionals for phase unwrapping," J. Opt. Soc. Am. A **12,** 2393–2400 (1995).
2. M. Rivera, J. L. Marroquin, M. Servin, and R. Rodriguez-Vera, "Fast algorithm for integrating inconsistent gradient fields," Appl. Opt. **36,** 8381–8390 (1997).
3. M. Takeda, H. Ina, and S. Kobayashi, "Fourier-transform method of fringe-pattern analysis for computer-based topography and interferometry," J. Opt. Soc. Am **4,** 156–160 (1982).
4. K. H. Womack, "Interferometric phase measurement using spatial synchronous detection," Opt. Eng. **23,** 391–395 (1984).
5. M. Rivera, "Robust phase demodulation of interferograms with open or closed fringes," J. Opt. Soc. Am. A **22,** 1170–1175 (2005).
6. D. J. Pugh and K. Jackson, "Automatic gauge block measurement using multiple wavelength interferometer," in *Contemporary Optical Instrument Design, Fabrication and Testing,* H. Beckmann, J. Briers, and P. R. Yoder, eds., Proc. SPIE **656,** 233–250 (1986).
7. G. Boensch, "Gauge blocks as length standards measured by interferometry or comparison: length definition, traceability chain, and limitations," in *Recent Developments in Optical Gauge Block Metrology,* J. E. Decker and N. Brown, eds., Proc. SPIE **3477,** 199–210 (1998).
8. G. Boensch, "Automatic gauge block measurement by phase stepping interferometry with three laser wavelengths," in *Recent Developments in Traceable Dimensional Measurements,* J. E. Decker and N. Brown, eds., Proc. SPIE **4401,** 1–10 (2001).
9. J. L. Marroquin, M. Rivera, S. Botello, R. Rodriguez-Vera, and M. Servin, "Regularization methods for processing fringe-pattern images," Appl. Opt. **38,** 788–795 (1999).
10. J. L. Marroquin, J. E. Figueroa, and M. Servin, "Robust quadrature filter," J. Opt. Soc. Am. A **14,** 779–791 (1997).
11. J. L. Marroquin, M. Servin, and R. Rodriguez-Vera, "Adaptive quadrature filters for multiphase stepping images," Opt. Lett. **23,** 238–240 (1998).
12. M. Rivera and J. L. Marroquin, "Adaptive rest condition potentials: first and second order edge-preserving regularization," J. Comput. Vision Image Understand. **88,** 76–93 (2002).
13. J. L. Marroquin, S. Mitter, and T. Poggio, "Probabilistic solution of ill-posed problems in computational vision," J. Am. Statist. Assoc. **82,** 76–89 (1987).
14. J. Villa, J. A. Quiroga, and M. Servin, "Improved regularized phase tracking technique for the processing of squared-grating deflectograms," Appl. Opt. **39,** 502–508 (2000).
15. R. Legarda-Saenz, W. Osten, and W. Juptner, "Improvement of the regularized phase tracking technique for the processing of nonnormalized fringe patterns," Appl. Opt. **41,** 5519–5526 (2002).
16. M. Rivera and J. L. Marroquin, "Half-quadratic cost functions for phase unwrapping," Opt. Lett. **29,** 504–506 (2004).
17. M. Servin, J. L. Marroquin, D. Malacara, and F. J. Cuevas, "Phase unwrapping using a regularized phase tracking system," Appl. Opt. **37,** 1917–1923 (1998).
18. M. Rivera, J. L. Marroquin, S. Botello, and M. Servin, "A robust spatio-temporal quadrature filter for multi-phase stepping," Appl. Opt. **39,** 284–292 (2000).
19. S. Geman and D. E. McClure, "Bayesian image analysis methods: An application to single photon emission tomography," in *Proceedings of the Statistical Computation Section* (American Statistical Association, 1985), pp. 12–18.
20. D. Geman and G. Reynolds, "Constrained restoration and recovery of discontinuities," IEEE Trans. Pattern Anal. Mach. Intell. **14,** 367–383 (1992).
21. D. Geman and C. Yang, "Nonlinear image recovery with half-quadratic regularization," IEEE Trans. Image Process. **4,** 932–946, (1995).
22. M. J. Black and A. Rangarajan, "Unification of line process, outlier rejection, and robust statistics with application in early vision," Int. J. Comput. Vision **19,** 57–91 (1996).
23. M. Rivera and J. L. Marroquin, "Efficient half-quadratic regularization with granularity control," J. Image Vision Comput. **21,** 345–357 (2003).
24. M. Proesmans, A. E. Pouwels, and L. Van Gool, "Couple geometry-driven diffusion equations for low level vision," in *Geometry-Driven Diffusion in Computer Vision,* B. M. ter Haar-Romeny, ed. (Kluwer Academic, 1994), pp. 191–228.
25. T. Tasdizen and R. Withaker, "Feature preserving variational smoothing of terrain data," in *Proceedings of the Second IEEE Workshop on Variational, Geometric and Level Set Methods in Computer Vision (VLSM'03)* (Institute of Electrical and Electronics Engineers, 2003), pp. 121–128.
26. J. M. Huntley, "An image processing system for the analysis of speckle photographs," J. Phys. E **19,** 43–49 (1986).
27. K. J. Gasvik, *Optical Metrology,* 3rd ed. (Wiley, 2002).
28. J. Nocedal and S. Wright, *Numerical Optimization,* Springer Series in Operational Research (Springer-Verlag, 1999).